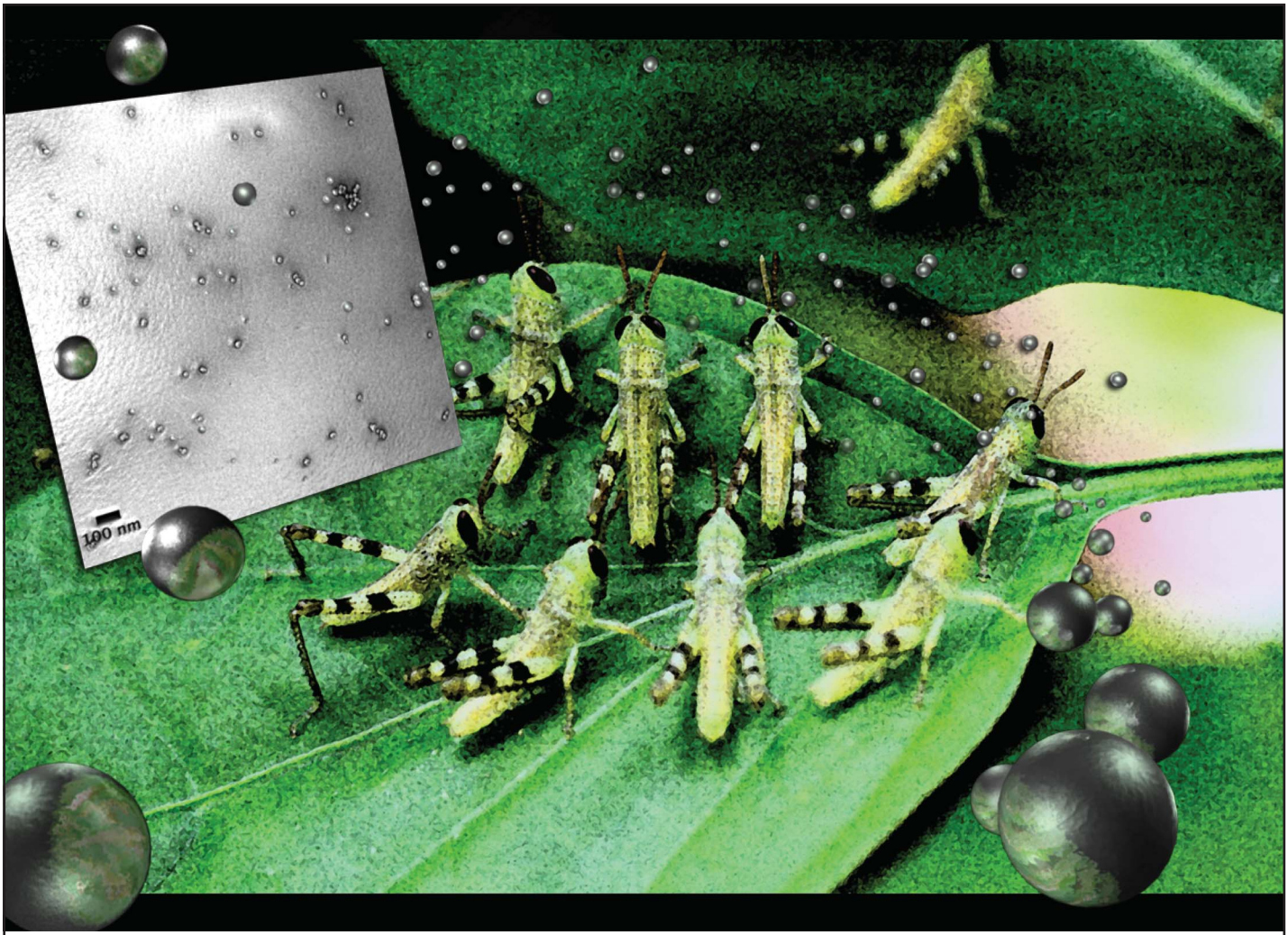

Showcasing research from Prof. Nathan C. Gianneschi's laboratory, the University of California, San Diego, USA.

Fluorogenic enzyme-responsive micellar nanoparticles

Enzymatic signalling cascades are utilized in living systems to communicate information through catalytic amplification. These cascades are implemented in all manner of biological events including swarming behavior in locusts. In our research, we are interested in how selective enzymatic reactions can be utilized to initiate assembly, aggregation, and disassembly of synthetic nanomaterials in a programmed fashion. Such processes have implications downstream in applications ranging from tissue targeting to advanced autonomous materials and sensors.

As featured in:

See Nathan C. Gianneschi *et al.*, *Chem. Sci.*, 2012, **3**, 2690.

RSC Publishing

www.rsc.org/chemicalscience

Registered Charity Number 207890

Chemical Science

Dynamic Article Links

Cite this: *Chem. Sci.*, 2012, **3**, 2690

www.rsc.org/chemicalscience

EDGE ARTICLE

Fluorogenic enzyme-responsive micellar nanoparticles†

Miao-Ping Chien, Matthew P. Thompson, Eugene C. Lin and Nathan C. Gianneschi*

Received 8th February 2012, Accepted 23rd May 2012
DOI: 10.1039/c2sc20165h

In this paper we describe enzyme-responsive fluorogenic micellar nanoparticles with detectable spectrophotometric properties unique to the particles and their aggregated state. These micelles are assembled from peptide–polymer amphiphiles (PPAs) labeled with either fluorescein or rhodamine. This is achieved by labeling otherwise similar block copolymer amphiphiles with each of the dyes. When mixed together, signals from the FRET-pairs can be utilized to detect particle assembly and hence enzymatic activity. Furthermore, we show FRET signals within the shell of the assembled micelles can be used to estimate particle stability (critical aggregation concentration) and enable a determination of intraparticle distances between amphiphiles in the micellar aggregates leading to elucidation of the packing arrangement of amphiphilic copolymers within the micelles.

Introduction

Enzymes are unique as biomarkers because they amplify detection events by catalytic turnover with selectivity that can be specific to given disease states.[1–4] The specificity and diversity of reactions catalyzed by enzymes and their importance as signal-amplifying biomarkers make them exceptionally attractive as tools in the assembly and manipulation of nanoscale materials.[5] In particular, nanoparticles capable of undergoing enzyme-programmed assembly, or morphology switches are of interest because unlike substrates such as fluorogenic oligopeptides, they can theoretically act as carriers of payloads that include specific molecular diagnostics and drugs. Although underutilized, enzymes have been harnessed as selective tools for the manipulation of nanoscale structures, a process that in itself constitutes a unique signaling event indicating enzyme activity.[5–9] Such responses have proven detectable based on routine morphology analyses *via* methods including electron microscopy and light scattering. However, changes in nanoscale architecture will only be detectable in more challenging settings (*e.g. in vivo*) if the action of the enzyme results in an output signal unique to the assembly, such as a spectrophotometric response. To enable this, we have developed peptide–polymer amphiphiles (PPAs)[10,11] linked to dyes[12] capable of undergoing efficient Förster Resonance Energy Transfer (FRET) for detecting structural properties and aggregation states of self-assembled enzyme-responsive nanoparticles. Herein, this concept is demonstrated for elucidation of particle stability, particle structure, and for monitoring enzyme-induced morphological transformations (Fig. 1).

Results and discussion

The PPAs utilized in these studies were designed as substrates for the cancer-associated enzyme, matrix-metalloproteinase 9 (MMP-9).[13–15] By utilizing this substrate as the polar head group of the copolymer, the micelle morphology and aggregation behaviour of the materials could be modified *via* peptide cleavage by MMP at the Gly–Leu peptide bond (Fig. 1). We reasoned that enzymatic reactions occurring within the shell of the particles

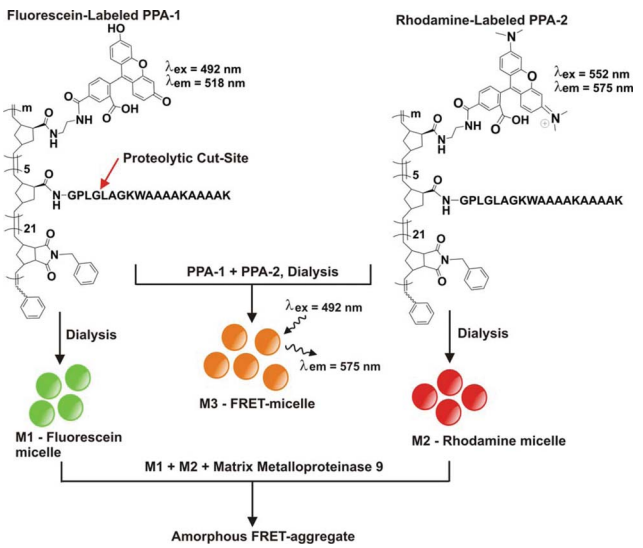

Fig. 1 Assembly of peptide–polymer amphiphiles (PPAs) to generate fluorogenic micellar nanoparticles. Polymers were labeled with peptides[4] and dyes, post-polymerization with block sizes determined by SEC-MALS analysis and spectroscopy. Degree of dye incorporation (*m*), was between 1 and 2 for both PPA-1 and PPA-2. See ESI for complete synthetic details†.

Department of Chemistry & Biochemistry, University of California, San Diego, La Jolla, CA, U.S.A. E-mail: ngianneschi@ucsd.edu

† Electronic supplementary information (ESI) available. See DOI: 10.1039/c2sc20165h

would facilitate a dramatic reduction in the hydrophilicity of the peptide-block, and would subsequently result in changes to the overall architecture *via* the establishment of new equilibria for surfactant aggregation. The polymers were synthesized using ring-opening metathesis polymerization[16,17] to generate block copolymers of a phenyl-modified norbornene as the hydrophobic block, a conjugatable NHS-ester for linkage through the amine terminus of the peptide, and a short block of primary amino-modified norbornene, for conjugation to dyes. As shown in Fig. 1, micelles of fluorescein labelled PPA-1 (**M1**) and rhodamine labelled PPA-2 (**M2**) were prepared by dialysis of solutions of the polymers in DMSO/DMF (1 : 1) against buffered water over 24 h (see ESI†). In addition, micelles were prepared from mixtures of the two PPAs to generate the FRET-micelle, **M3**.

We aimed to develop a method that allows an accurate determination of the arrangement of polymeric amphiphiles packed within micelles and to monitor structural changes induced by responses to enzymes. Moreover, this method should be amenable to use in complex environments where other particulates may be present. Such solutions containing mixtures of particles are not easily amenable to analysis by light scattering or TEM image analysis. We determined that the distance dependence of FRET efficiency of appropriately paired dyes would provide such a route and indeed, has been extensively utilized in biochemical systems.[18–21] However, the use of FRET efficiency for elucidating structural parameters in supramolecular self-assembled systems has been surprisingly limited, despite its great potential in determining solution phase structures of multicomponent assemblies.[21] Relevant and notable exceptions involve the use of fluorescence energy transfer for studying interfacial regions in the assembly of nanoparticles and micelles.[22–24] Here, we demonstrate that in addition to enabling a direct measurement of exceptionally low CAC for micelles, and a geometrical determination of aggregation number,[23,25] FRET-labeled PPAs can be utilized to sensitively monitor micellar nanoparticle response to enzymes. These parameters were determined by analysis of the distance dependence of FRET efficiency within polymeric micelles in which each amphiphile in the assembly is covalently end-labeled with one of two dyes in a pair. The result is micellar aggregates with dyes displayed on their surfaces.

Initially, the fluorescence spectra and efficiency of FRET for a range of concentrations of PPA-1 and PPA-2 in the formation of micelles was studied (Fig. 2). **M1**, **M2** and **M3**, are 35–40 nm in diameter as characterized by TEM (Fig. 2a for **M3**) and by DLS (Fig. 2b). The two single dye labeled micelles have the expected spectroscopic properties, with a peak due to fluorescein at 512 nm for **M1** and no observable fluorescence upon excitation at 470 nm for **M2** (Fig. 2c). However, blending PPA-1 and PPA-2 to form **M3** provides a mixed dye micelle with fluorescent properties indicative of a FRET pair within the Förster radius as evidenced by rhodamine fluorescence observable at 563 nm. At PPA concentrations above 1 μM we found that the ratio of the intensities of each peak maximum (I_{563}/I_{512}) is constant. This indicates the maximum FRET efficiency possible for this system (Fig. 2d). However, upon dilution of **M3** over the range from 2.5 μM to 2 nM, a greater decrease in intensity of the peak at 563 nm (rhodamine) compared to 512 nm (fluorescein) is observed. Therefore, a CAC of 8 nM is assigned for **M3** as the

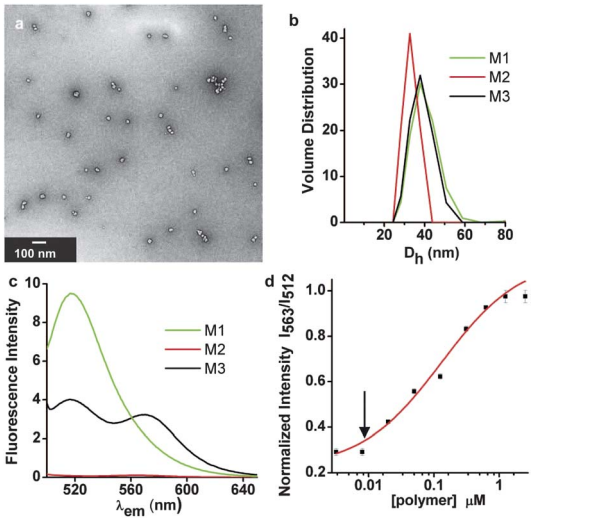

Fig. 2 TEM, DLS and fluorescence spectroscopy of fluorogenic micelles. a) TEM of 30 nm **M3**. b) DLS of **M1**, **M2** and **M3** showing hydrodynamic diameters (D_h) in the range of 30–40 nm. c) Fluorescence emission spectra of **M1**, **M2** and FRET-micelle, **M3** upon excitation at 470 nm. d) Ratio of normalized emission intensity for maxima at 563 nm (rhodamine) and 512 nm (fluorescein) over a range of concentrations of PPA-1 and PPA-2 upon excitation at 470 nm. Arrow indicates onset of detectable FRET.

concentration at which the onset of a detectable FRET signal is observed. This is a generalizable approach providing, in this case, an exceptionally sensitive and direct method for determining CAC. Such a labeling strategy for observing intact particles is especially useful in cases where they are particularly stable, limiting the utility of standard CAC determination assays using non-covalently associated solvochromatic dyes where the limit of detection is significantly above CAC. Indeed, we have had no success implementing standard assays with regards to these systems and gathering accurate data at low concentrations. Direct labeling of the polymers also means they can be observed in complex milieu without the need for additional dye additives as will be highlighted in the context of enzymatic studies (*vide infra*).

In addition to determining particle stability, we sought to utilize the direct labeling strategy to elucidate structural features of the micelles. It has been shown that, if micelles are assumed to be assemblies of amphiphiles packed as cones with spherical bases, then the maximum integer number of amphiphiles in a micelle (N_{sph}) can be directly calculated if the angle at the vertex of each cone (α) is known (equation in ESI†).[26] We hypothesized that the angle α could be directly determined knowing the distance (r) between fluorescein and rhodamine, that are assumed to be located at the centers of each cone (or copolymer amphiphile) in a spherical micelle (Fig. 3). The angle at the vertex (α) may be found *via* simple trigonometry because r is a chord between the centers of each spherical-based cone packed within micelles of radius, R. It follows that with experimentally measured values for R (TEM) and r (by FRET analysis), α can be calculated. Therefore, we assume that polymeric amphiphiles are close-packed cones that are not diffusing with respect to each other but are instead confined in restricted dimensions on the length scale relevant to FRET.[22] Finally, each cone is end-labeled

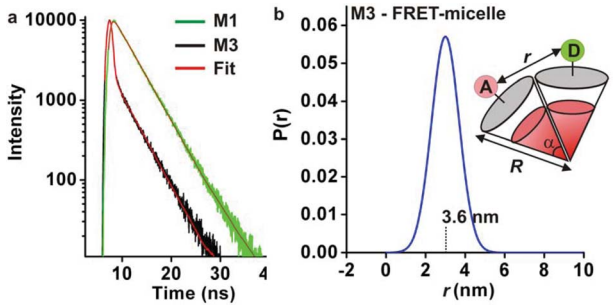

Fig. 3 Time-domain fluorescence intensity decay analysis of **M1** and **M3** for determination of structural parameters. a) Fluorescence lifetime of **M3** and **M1** fit to a distance distribution function, and single exponential respectively (red lines) giving $t_D = 3.98 \pm 0.01$ ns (from **M1** data) for unquenched fluorescein. b) For **M3**, a range of distances between donor and acceptor (D and A) is considered, expressed as a probability function $P(r)$. The mean distance, 3.6 nm, can in turn be used to determine $t_{DA} = 0.29$ ns. Radius (R) of the micelles was determined by TEM (Fig. 2).

with donor or acceptor dyes that have fast rotational motion on the timescale of FRET.

The donor–acceptor (D–A) distance distribution was determined by analyzing the time-domain intensity decay of the donor (Fig. 3a).[21] Therefore, we fit the data as a summation of donor decays for all accessible D–A distances (Fig. 3b, and ESI†). For **M3**, we have $R = 15$ nm, and $r = 3.6$ nm $\pm$ 0.6, giving $\alpha = 14° \pm 2$. Thus, we calculate $N_{sph} = 241 \pm 60$, taking account of the distribution about the mean distance between the donor and acceptor. This geometrically derived maximum aggregation number compares favorably with that determined from average particle molecular weight in solution by static light scattering (SLS) analysis of **M3**, which yields a weight average $N_{agg} = 209 \pm 0.82$. Furthermore, SLS was used to determine N_{agg} of 159 ± 0.34 for **M1**, and 304 ± 2.3 for **M2**. It is clear that these values are on the same order, as expected for similar surfactants generating similar sized micellar nanoparticles. Indeed, the order of this aggregation number for this class of surfactant could be corroborated by counting particles in TEM images whereby the number of micelles per L was determined by mixing them with a stock solution of 20 nm gold nanoparticles (see ESI†). This FRET approach therefore provides a viable method for monitoring particle assembly and detailed structural features in PPA assemblies without requiring TEM or SLS.

PPA-1 and PPA-2 were designed as substrates for MMPs. Therefore, we sought to study enzyme-induced rearrangement of the micelles, aiming to analyze the process *via* fluorescence spectroscopy in buffer solutions (Fig. 4). Furthermore, to demonstrate the utility of FRET in analyzing micelle behavior in biological milieu, we examined their response to MMP-9 in blood serum doped samples of cell-growth media. Initial experiments were conducted to study enzyme kinetics on the micelle-based substrates (see ESI†). These were conducted by preparing a micelle from a PPA, end-labeled with fluorescein and conjugated to a peptide labeled with Dabcyl as a quencher, that when cleaved resulted in an ON-switch of fluorescence. These studies confirm that kinetics were similar on both particle-linked substrates and simple oligopeptide substrates. Next, we mixed **M1** and **M2** together with purified, commercial MMP-9 and

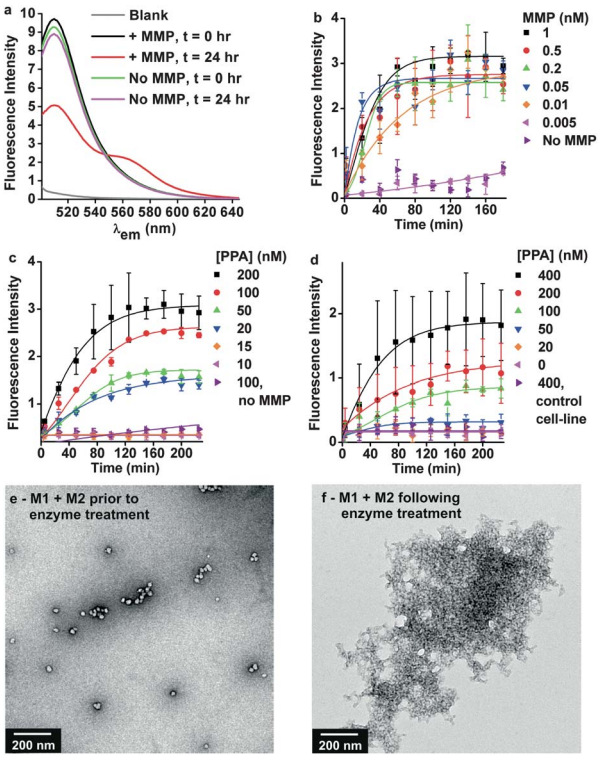

Fig. 4 Response of mixtures of **M1** and **M2** to MMPs. a) Fluorescence spectra of **M1** and **M2** (0.5 μM each with respect to PPA) with and without MMP-9 (10 nM) at times indicated following enzyme addition; $\lambda_{ex} = 470$ nm. b–d) Fluorescence intensity *vs.* time plots *via* plate reader analysis, to monitor rearrangement of PPA-1 and PPA-2 into new FRET active aggregates; $\lambda_{ex} = 490$ nm and $\lambda_{em} = 590$ nm. b) Detection of MMP-9 down to 10 pM of enzyme with **M1** and **M2** (at 0.5 μM, [PPA]). c) Detection of MMP-9 at 10 nM with varying concentrations of **M1** and **M2** shown with respect to [PPA], detectable down to 20 nM of polymer. d) Detection of cell-secreted (WPE1-NA45 cells) MMP-2 and -9 with varying concentrations of **M1** and **M2** shown with respect to [PPA]. Cells were seeded at 1.6×10^4 cells/well in a clear bottom 96-well plate in DMEM. After 24 h, cell medium was added to solutions of **M1** and **M2**. MMP-2 and -9 were at 0.048 nM and 0.005 nM respectively as quantified by an ELISA assay (see ESI†). Control was the non-MMP expressing MCF-7 cell-line cultured in the same manner. All reactions run in PBS, unless otherwise noted. e–f) TEM of **M1** and **M2** before and after 24 h following MMP-9 treatment.

observed the emission spectra over time (Fig. 4a) showing the formation of a new FRET-active species in solution as PPAs are cleaved and rearrange into aggregates containing both dyes. We note that peptide cleavage rates and formation of the new FRET signal, indicating aggregate formation, are similar and therefore consistent with them being concomitant processes. The peptide fragments could be quantified by HPLC (41% cleavage efficiency after 24 h), and characterized by MALDI (see ESI†). This low efficiency may be due to steric hinderance within the particle shells, or within the aggregates as they form during the reaction. Despite this, the particles are sufficiently susceptible to allow a complete shift to the aggregated species as evidenced by DLS (see ESI†). Furthermore, the FRET efficiency calculated from donor lifetimes is comparable to, but is reduced for these aggregates (efficiency = 85%) compared to **M3** (efficiency = 93%). In addition, the relative inhomegeneity of the aggregates

compared to the control particles (**M3**) is observed by comparison of ratios of donor and acceptor intensities in Fig. 2c (1 : 0.8) *vs.* Fig. 4a (1 : 0.43). This is consistent with a less homogeneous distribution of donors and acceptors. Despite this slight decrease in FRET efficiency, the response is clearly observable down to 10 pM of MMP-9 for solutions containing 0.5 μM of micelles (Fig. 4b – concentration of micelles is with respect to PPA in each case). Furthermore, MMP-9 at 10 nM is observable down to 20 nM of PPA (Fig. 4c), a result that is consistent with the exceptional stability of these aggregates with CACs in the range of 10 nM. In addition, **M1** and **M2** underwent enzyme-induced aggregation when treated with a mixture of expressed MMPs (Fig. 4d). We note that these particles were designed to be responsive to both cancer-associated enzymes MMP-2 and MMP-9 as expected for the substrate sequence chosen. These experiments were performed by treating **M1** and **M2** with cell growth media containing MMPs excreted over 24 h from WPE1-NA45 cells, and present at 0.048 nM and 0.005 nM (MMP-2 and -9 respectively) as determined by a quantitative ELISA assay (see ESI†). In this case, substrate concentrations of 100 nM (with respect to PPAs) resulted in observable responses within 4 h reaction time. Finally, this enzyme-induced rearrangement of PPAs was characterized by TEM, confirming the formation of a new aggregated species upon cleavage of the peptide sequence in **M1** and **M2** (Fig. 4e–f, see ESI† for **M3** + MMP-9). It is this aggregated species that carries both dyes, in close enough proximity to allow spectroscopic characterization by FRET. To demonstrate the utility of the labeling approach in the detection of enzymes in more complex media, we mixed **M1** and **M2** in blood serum doped cell media samples and treated them with MMP-9 (Table 1). This resulted in an easily detectable and significant shortening of the fluorescence lifetime.

Conclusions

We have described nanoparticles that undergo enzyme-induced changes in structure which are detectable in complex environments. This is a necessary step in the future implementation of enzyme-programmed materials in *in vivo* applications. In particular, where enzymatic signals are specific to given disease states including inflammation and metastasis.[14] This is enabled by a labeling approach that provides critical information regarding particle structure and stability. Together, these studies are consistent with exceptionally stable micelles that show no detectable scrambling of PPAs when mixed together in the absence of MMP. Moreover, the enzymatic response constitutes a novel approach to the detection of enzymes whereby the stimulus induces detectable changes in nanoparticle morphology. We note that this is not intended as a technology towards sensitive diagnostic detection of enzymes *in vitro*, but rather for analyzing and utilizing the response of nanomaterials to enzymes as they undergo complex changes in structure.[27] Furthermore, by detecting changes in fluorescence lifetime induced by rearrangement of appropriately labeled polymers, these processes can be observed in complex milieu. We propose that this type of FRET-pair labeling strategy will be generally useful to those wanting to monitor particle aggregation state in complex environments, where light scattering and electron microscopy suffer deleterious interference from other particulates and detritus. We are currently examining this labeling approach for its utility in monitoring the response of nanoparticles to disease-associated enzyme activity *in vivo*.

Table 1 Detection of MMP-9 at 10 nM in blood serum doped DMEM, cell growth medium

Micelle[a]	MMP-9	Solution conditions[b]	Fluorescence lifetime, t (ns)
M1	–	20% serum	3.94 ± 0.03
M1	+	20% serum	3.93 ± 0.01
M1 + M2	–	20% serum	3.93 ± 0.01
M1 + M2	+	20% serum	0.56 ± 0.02
M1 + M2	+	no serum	0.59 ± 0.01

[a] Micelle concentrations for **M1** and **M2** are 0.1 μM, and 1 μM respectively, with respect to PPA concentration. [b] Micelles were incubated under these conditions at 37 °C for 24 h prior to measuring lifetimes. DMEM = Dulbecco's Modified Eagle Media. Detection of MMP in blood serum doped DMEM media *via* significant shortening in fluorescence lifetime indicating particle fusion upon cleavage of PPAs within **M1** and **M2**.

Acknowledgements

The authors acknowledge support for this program from AFOSR through a PECASE (FA9550-11-1-0105). In addition, we acknowledge support from ARO (W911NF-11-1-0264). Furthermore, we thank NIH (NIBIB) for their generous support (1R01EB011633) and *via* a NIH Director's New Innovator Award (1DP2OD008724). N.C.G. acknowledges the Henry & Camille Dreyfus Foundation for a New Faculty Award. E.C.L. acknowledges support from NIBIB (P41EB002031). We thank Prof. Akif Tezcan for his insights and helpful suggestions.

Notes and references

1 R. K. Saiki, S. Scharf, F. Faloona, K. B. Mullis, G. T. Horn, H. A. Erlich and N. Arnheim, *Science*, 1985, **230**, 1350–1354.
2 E. Engvall and P. Perlmann, *Immunochemistry*, 1971, **8**, 871–874.
3 L. Zhu and E. V. Anslyn, *Angew. Chem., Int. Ed.*, 2006, **45**, 1190–1196.
4 T. Jiang, E. S. Olson, Q. T. Nguyen, M. Roy, P. A. Jennings and R. Y. Tsien, *Proc. Natl. Acad. Sci. U. S. A.*, 2004, **101**, 17867–17872.
5 M. E. Hahn and N. C. Gianneschi, *Chem. Commun.*, 2011, **47**, 11814.
6 G. Von Maltzahn, T. J. Harris, J.-H. Park, D.-H. Min, A. J. Schmidt, M. J. Sailor and S. N. Bhatia, *J. Am. Chem. Soc.*, 2007, **129**, 6064–6065.
7 T. H. Ku, M. P. Chien, M. P. Thompson, R. S. Sinkovits, N. H. Olson, T. S. Baker and N. C. Gianneschi, *J. Am. Chem. Soc.*, 2011, **133**, 8392–8395.
8 R. J. Amir, S. Zhong, D. J. Pochan and C. J. Hawker, *J. Am. Chem. Soc.*, 2009, **131**, 13949–13951.
9 R. V. Ulijn, *J. Mater. Chem.*, 2006, **16**, 2217–2225.
10 H. Cui, M. J. Webber and S. I. Stupp, *Peptide Sci.*, 2010, **94**, 1.
11 C.-L. Chen, P. Zhang and N. L. Rosi, *J. Am. Chem. Soc.*, 2008, **130**, 13555–13557.
12 H. A. Behanna, K. Rajangam and S. I. Stupp, *J. Am. Chem. Soc.*, 2007, **129**, 321–327.
13 K. Kessenbrock, V. Plaks and Z. Werb, *Cell*, 2010, **141**, 52–67.
14 R. L. Scherer, J. O. McIntyre and L. M. Matrisian, *Cancer Metastasis Rev.*, 2008, **27**, 679–690.
15 D. G. Vartak and R. A. Gemeinhart, *J. Drug Targeting*, 2007, **15**, 1–20.
16 T. M. Trnka and R. H. Grubbs, *Acc. Chem. Res.*, 2001, **34**, 18–29.
17 D. Smith, E. B. Pentzer and S. T. Nguyen, *Polym. Rev.*, 2007, **47**, 419–459.

18 L. Stryer, *Annu. Rev. Biochem.*, 1978, **47**, 819–846.
19 R. M. Clegg, *Methods Enzymol.*, 1992, **211**, 353–388.
20 P. R. Selvin, *Nat. Struct. Biol.*, 2000, **7**, 730–734.
21 J. R. Lakowicz, *Principles of Fluorescence Spectroscopy*, 1983.
22 J. P. S. Farinha and J. M. G. Martinho, *J. Phys. Chem. C*, 2008, **112**, 10591–10601.
23 K. Schillen, A. Yekta, S. Ni, J. P. S. Farinha and M. A. Winnik, *J. Phys. Chem. B*, 1999, **103**, 9090–9103.
24 J. P. S. Farinha, K. Schillen and M. A. Winnik, *J. Phys. Chem. B*, 1999, **103**, 2487–2495.
25 T. J. V. Prazeres, M. Beija, M.-T. Charreyre, J. P. S. Farinha and J. M. G. Martinho, *Polymer*, 2010, **51**, 335–367.
26 S. Tsonchev, G. C. Schatz and M. A. Ratner, *Nano Lett.*, 2003, **3**, 623–626.
27 S. Samarajeewa, R. Shrestha, Y. Li and K. L. Wooley, *J. Am. Chem. Soc.*, 2012, **134**, 1235–1242.

